Sensors and Actuators A 312 (2020) 112090

Contents lists available at ScienceDirect

Sensors and Actuators A: Physical

journal homepage: www.elsevier.com/locate/sna

3D printed, modularized rigid-flexible integrated soft finger actuators for anthropomorphic hands

Ningbin Zhang[a], Lisen Ge[a], Haipeng Xu[a], Xiangyang Zhu[a,b,*], Guoying Gu[a,b,*]

[a] Robotics Institute, School of Mechanical Engineering, Shanghai Jiao Tong University, Shanghai 200240, China
[b] State Key Laboratory of Mechanical System and Vibration, Shanghai Jiao Tong University, Shanghai 200240, China

ARTICLE INFO

Article history:
Received 8 March 2020
Received in revised form 8 May 2020
Accepted 19 May 2020
Available online 30 May 2020

Keywords:
Rigid-flexible integrated soft finger actuator
Pneumatical bellow structure
Anthropomorphic hand
Multi-material 3D printing
Modular design and fabrication

ABSTRACT

Owing to the integrated muscular, ligamentous and skeletal structures and coupled degrees of freedom (DoFs), it is a long-term challenge in the field of robotics to design an anthropomorphic hand that mimics the biological structures and dexterous motions of human hands. In this paper, we present pneumatical, multi-material 3D-printed, modularized rigid-flexible integrated soft finger actuators (RFiSFAs) that can be directly assembled to an anthropomorphic hand. First, we introduce the mechanism of the RFiSFA with a pneumatic bellow chamber and a joint structure, and investigate the influence of the chamber material and the bellow number on the flexion angles and output forces performances of the RFiSFA. Next, we design and fabricate a 2-DoF flexion finger with two serial RFiSFAs and a 3-DoF thumb with two serial RFiSFAs and two parallel RFiSFAs. Then, we perform tests to characterize the motion and force performance of the fingers and thumb. Finally, we integrate and assemble an 11-DoF anthropomorphic hand with four flexion fingers and one thumb, and experimental results demonstrate the capability of the hand in grasping objects with different dimensions, shapes and textures.

1. Introduction

Over countless generations, our hands have evolved integrated muscular, ligamentous and skeletal structures to perform dexterous movements with coupled DoFs, which motivates inventors and scientists to create various anthropomorphic hands in the field of robotics [1]. The success of these anthropomorphic hands, however, mostly introduces complex rigid and flexible components by integrating numbers of motors, linkages, transmission gears, tendons, connectors, electronic boards and controllers, usually with years of development for each prototype [2]. To simplify the structure and achieve rapid prototyping of anthropomorphic hands, some minimalist and useful approaches are developed, such as underactuation [3–5], synergies [4,6–8] and soft robotics [5,9–11].

Among these approaches, soft robotics renders the anthropomorphic hand distinctive features of inherent compliance and impact resistance with the involvement of soft functional materials, which is partially or difficultly achieved by other approaches. Based on soft robotics, numerous "soft hands" are designed and fabricated ranging from the single-finger grippers to the multi-finger anthropomorphic hands [12–17]. Most soft hands have been designed with fingers integrating self-contained elastomeric actuators and deformable structures, which are generally manually fabricated by replica molding process and its variant approaches. The fabricated fingers are furtherly manually assembled with other flexible or rigid components. However, both fabrication and assembly process are laboriously intensive, and may be not suitable for scenarios requiring compact design and high consistency. To address these issues, three-dimensional (3D) printing is utilized to create monolithic soft fingers or hands [18–20] with single flexible material. However, it is difficult to fully replicate the articular motions of the human finger which is induced by large stiffness variations between biological joints and skeletons. To overcome the stiffness limitation due to single material, multiple materials with a wide range of constituent moduli are introduced into the 3D printing process for constructing robotic systems or components, including multilegged robots [21–23], combustion-powered jumpers [24], end effectors [25], soft actuators [2627] and hybrid stiffness-tunable robots [28]. Recently, the multi-material 3D printing approach is employed for fabricating hand's flexible joints and rigid skeletons. For example, as presented in [29], a soft skeleton hand with passive joint and skeleton motions is designed and fabricated to perform piano music. However, there is no active actuation modules in the development. To the best of our knowledge, there is rare study to

* Corresponding authors at: Robotics Institute, School of Mechanical Engineering, Shanghai Jiao Tong University, Shanghai 200240, China.
E-mail addresses: mexyzhu@sjtu.edu.cn (X. Zhu), guguoying@sjtu.edu.cn (G. Gu).

https://doi.org/10.1016/j.sna.2020.112090
0924-4247/

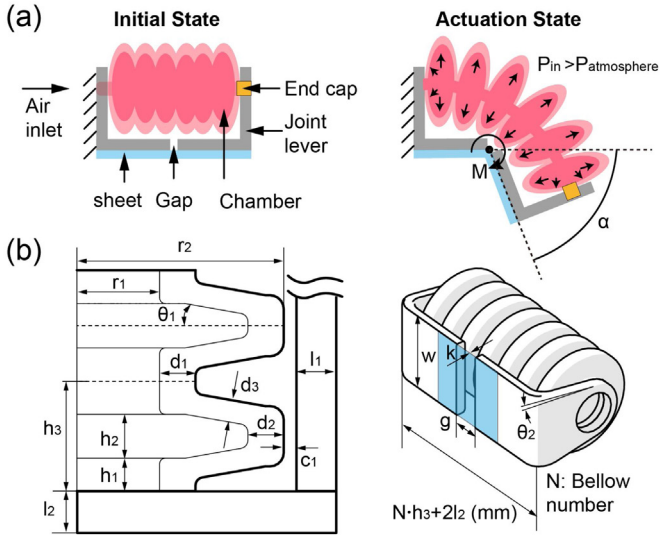

(c)

Parameter	Value (mm)
d_1	1.3
d_2	1.3
d_3	0.8
r_1	3
r_2	8.06
h_1	1.2
h_2	1.6
h_3	4
c_1	0.5
l_1	1.5
l_2	1.5
w	8.6
g	3
k	0.2
Parameter	**Value (°)**
θ_1	10
θ_2	10

Fig. 1. Schematic illustration of the RFiSFA. (a) Structure and actuation mechanism. (b) Dimension parameters. (c) Parameter values.

develop 3D-printed anthropomorphic hands with active and multiple DoFs. The challenges not only lie in designing bioinspired finger actuators with rigid-flexible features, but also in decoupling hand DoFs and reconstructing them in a confined space.

In this paper, we propose the multi-material, 3D-printed pneumatic actuators with rigid-flexible features, termed as RFiSFAs, to directly generate an anthropomorphic hand in a modularized manner (see movie S1 for an illustration). The RFiSFA has a bioinspired, hybrid structure integrating a pneumatic bellow chamber and joint skeletons. We firstly investigate the influence of the chamber material and the bellow number on the flexion angles and output forces performances of the RFiSFA. After that, we present the design and fabrication of two classes of fingers: 2-DoF flexion fingers with two serial RFiSFAs and 3-DoF thumb with two serial RFiSFAs and two parallel RFiSFAs. Furtherly, we characterize the motion and force performance of the fingers and thumb based on the prototype testing. Finally, we develop an 11-DoF anthropomorphic hand with one thumb and four flexion fingers. The experimental results show that the fabricated hand is robust against proper hammer strike and capable of grasping objects with different dimensions, shapes and textures under pneumatic control.

The main contribution of this paper is summarized as follows:

(1) We design and fabricate modularized, pneumatically actuated RFiSFAs through multi-material 3D printing;
(2) We develop an 11-DoF anthropomorphic hand with one thumb and four fingers made of 12 RFiSFAs.
(3) We evaluate the motion and force performance of the fingers and the dexterity of the hand.

The remainder of this paper is organized as follows. Section 2 demonstrates the design of the RFiSFA. Section 3 presents the modular design and fabrication of the multi-DoF fingers based on the RFiSFAs for an anthropomorphic hand. Section 4 characterizes the motion and force performance of the fingers. This section also presents the mobility, dexterity and robustness of the fabricated 11-DoF anthropomorphic hand. The conclusions and future work are presented in Section 5.

2. Design of the RFiSFA

2.1. The structure and the actuation mechanism

The motion of human hand can be approximately regarded as coupled motions of multiple joint rotations [30]. Based on this fact, we design RFiSFA as 1-DoF active joint to perform analogous motions. As shown in Fig. 1(a), an RFiSFA consists of a hollow, flexible bellow-type chamber and two rigid joint levers connected by a flexible but inextensible sheet. An air inlet and an end cap are designed for pneumatic connection and blocking, respectively. Upon pressurization, the bellow-type chamber extends along the axial direction and is constrained by the joint structure, thus generating the flexion angle α and the output torque M. The flexion angle and the output torque of the RFiSFA are not only related to the supplied air pressure, but also to materials and structural dimensions [31]. In general, the selections of the used materials depend on the 3D printing system, which will be illustrated in Section 2.2. The dimension parameters and their values are shown in Fig. 1(b) and (c), respectively. Note that the length of RFiSFA is calculated by Nh_3+2l_2, where N is the bellow number. Some other parameters are designed considering the dimensions of human finger joints, such as the width ($2r_2 = 16.12$ mm) and the height ($l_1+c_1+2r_2 = 18.12$ mm) of the RFiSFA. The cross-section of the chamber is non-uniformly designed (d_1=$d_2 = 1.3$ mm, $d_3 = 0.8$ mm) to reduce stress concentration and enhance working stroke simultaneously [21,31]. The inner radius of the chamber ($r_1 = 3$ mm) should be designed as large as possible for rapid removing of the supporting material. In this work, we focus on investigating the effect of the chamber material and the bellow number on the performances of RFiSFA s while other parameters are set to be constant for simplicity.

2.2. The selection of the chamber material

We use the Polyjet 3D printer (J750, Stratasys Ltd., USA) and the GrabCAD Print software (version 1.28.16.50383) to fabricate the RFiSFA. This printing system provides two basic series of materials including Vero series (rigid) and Agilus30 (flexible), and numerous interpolated materials which are termed as Agilus30-Vero digital

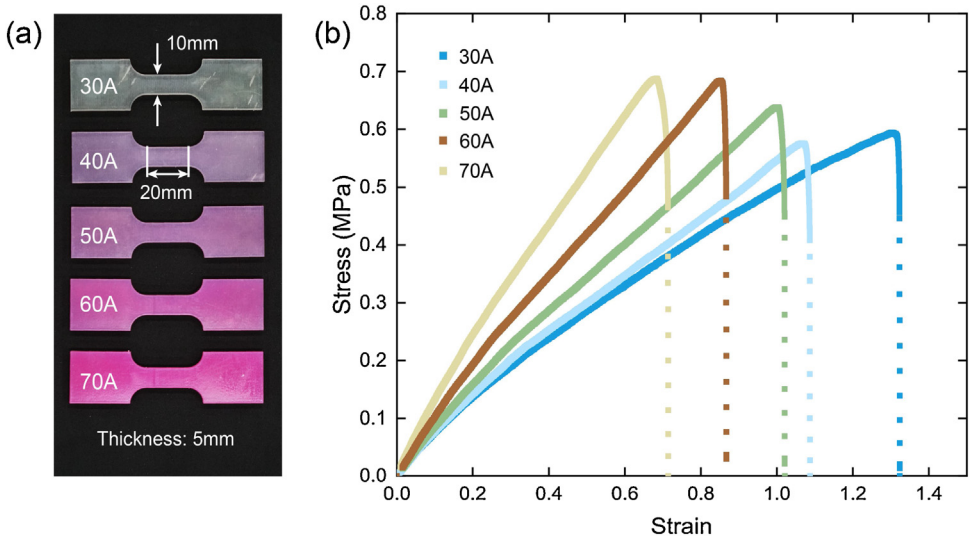

Fig. 2. Characterization on the mechanical properties of the printing materials. (a) Customized specimens with different hardness for tensile tests. (b) Mean stress ($n = 3$) of the specimens plotted as a function of the strain.

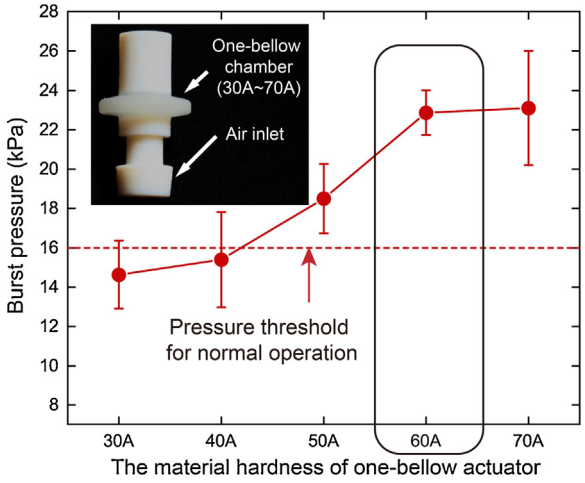

Fig. 3. Mean burst pressure ($n = 3$) and the standard deviation plotted as a function of the material hardness of one-bellow actuator.

materials. Their fundamental mechanical properties can be found in [32].

To select a proper material for the chamber, we firstly perform uniaxial tensile tests to investigate the mechanical properties of five printing materials in the used 3D printer, including pure Agilus30 (hardness = 30A) and Agilus30-Vero digital materials (hardness = 40A, 50A, 60A, 70A). In this test, the ZwickRoell Materials Testing System (Model Z0020) is used with a tensile speed of 10 mm/min. The specimens of different materials are shown in Fig. 2(a) and their stress-strain curves are shown in Fig. 2(b). The results indicate that an increase of material hardness results in an increase of the maximum stress (also the Young's module), while a decrease of the maximum strain. Therefore, we should make a tradeoff between the maximum stress and the stroke. As an example, we design and fabricate a series of one-bellow actuators without joint structures to measure their burst pressures (Fig. 3). We may mention that all the dimension parameters of a one-bellow chamber are in accordance with those corresponding parts of the RFiSFA. In the test, we connect the actuators to the air source controlled by the air regulator (ITV2050−312BL, SMC Inc., Japan) and inflate the actuators with 2 kPa pressure increments until they burst. The recorded burst pressures are shown in Fig. 3. The results indicate that with the increase of material hardness, the actuator burst pressure increases. Particularly, the burst pressures of 60A and 70A actuators are almost the same (22.9 kPa vs. 23.1 kPa). However, the standard deviation (SD) of 60A actuator is smaller than that of the 70A (1.1 kPa vs. 2.9 kPa). Therefore, we select 60A material in this work to fabricate the chamber and set a pressure limit of 16 kPa for the RFiSFA.

2.3. The selection of the bellow number

In the following, we will investigate the bellow number on the influences of the flexion angle, the blocking force, and the chamber length of RFiSFAs.

To this end, we fabricate a series of RFiSFAs with different bellow numbers (i.e. 6, 7, 8, 9,10, and 11). The fabrication steps are similar to those of the one-bellow actuators. The only difference is that a flexible but inextensible sheet is required to connect two joint levers. In this work, we attach a tailored non-woven fabric (0.2 mm in thickness) to the joint levers with the glue (A401, Ausbond Ltd., China) to realize reliable joint structures.

Then, we measure the flexion angle of each RFiSFA under supplied pressures. As shown in Fig. 4(a), the RFiSFA is mounted on a base and can flex freely. We attach 2 markers on the proximal lever and 2 markers on the distal lever, respectively. The flexion angles are calculated based on the relative positions of the markers, which is captured by two cameras (6D, Canon Ltd., USA). The *Stereo camera calibration* tool in Matlab 2018a is used for camera calibration. The results in Fig. 4(b) show that an increase of the bellow number results in an increase of the flexion angle of each RFiSFA. The maximum flexion angle is $47.3 \pm 0.82^\circ$ for the 6-bellow RFiSFA and $99.0 \pm 4.24^\circ$ for the 11-bellow RFiSFA under the supplied pressure of 16 kPa.

Next, we measure the blocking force of the RFiSFA with different bellow number. Fig. 5(a) shows the measurement setup (taking the 11-bellow RFiSFA as an example). The proximal end of RFiSFA is fixed on a platform and the tip is regulated in contact with the load cell (ME K3D120, ME-Messsysteme Ltd., Germany). Upon pressurization, the motion of the RFiSFA is blocked by another constraint platform and the blocking force is recorded. The results in Fig. 5(b) show that an increase of bellow number results in an increase of blocking force. The maximum blocking forces are 0.33 ± 0.01 N for

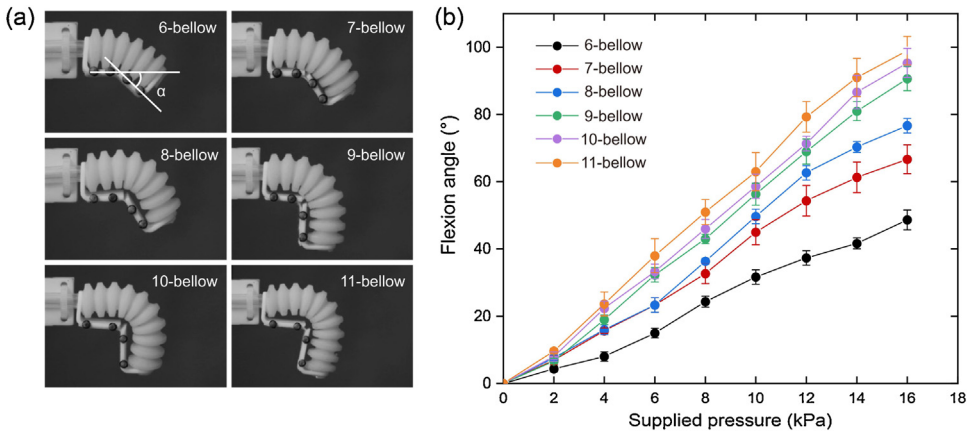

Fig. 4. Characterization of the flexion angle of the RFiSFAs with different bellow number. (a) Still images of RFiSFAs with different bellow numbers at 16 kPa. (b) Flexion angle plotted as a function of the supplied pressure. Error bars represent standard deviation over $n = 3$ trials.

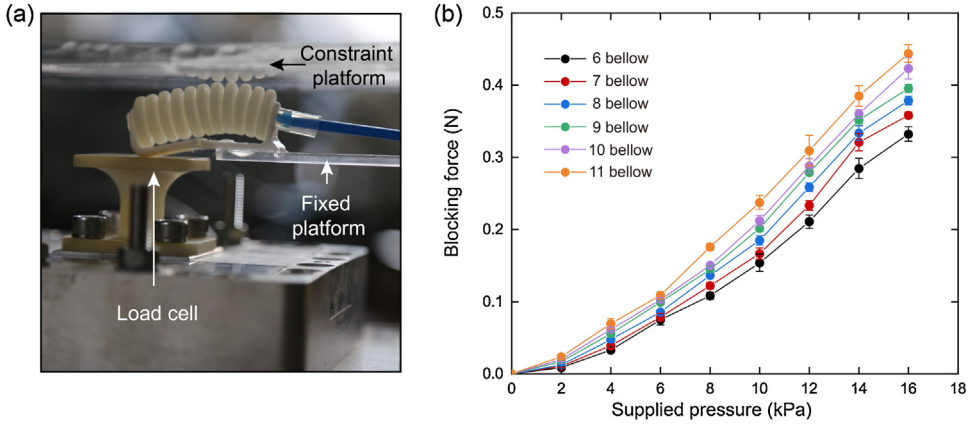

Fig. 5. Characterization of the blocking force of the RFiSFAs with different bellow number. (a) Experimental setup. (b) Blocking force plotted as a function of the supplied pressure. Error bars represent standard deviation over $n = 3$ trials.

the 6-bellow RFiSFA and 0.44 ± 0.01 N for the 11-bellow RFiSFA under the supplied pressure of 16 kPa.

The above experimental results demonstrate that both the flexion angle and the blocking force become larger with the increase of the bellow number. Due to the limited space in an anthropomorphic hand, a tradeoff between the maximum flexion angle/maximum blocking force and the chamber length should be made. In the current work, we should design two kinds of RFiSFAs for the anthropomorphic hand. The first RFiSFA is used to drive the metacarpophalangeal (MCP) joint, the proximal interphalangeal (PIP) joint or the joint for thumb adduction whose maximum flexion angles should be within 60° to 90° [30]. The second RFiSFA is used to drive the joint for thumb circumduction whose maximum flexion angle should be larger than 90° [30]. To select proper bellow numbers for these two RFiSFAs, we plot the maximum flexion angle and the chamber length as a function of the bellow number (Fig. 6). The design spaces of the maximum flexion angle and the chamber length are colored with grey and red, respectively. Therefore, we select the bellow number for the first RFiSFA (Fig. 6(a)) and second RFiSFA (Fig. 6(b)) as 7 bellows and 10 bellows, respectively.

Finally, to validate the performance of chamber, we characterize the flexion angle and the blocking force for the selected RFiSFAs under the constant supplied pressure of 16 kPa (total 12 h with a step of an hour). As shown in Fig. 7, the flexion angles of both RFiSFAs increase in the first several hours (0–7 t h hour for the 7-bellow one and 0–9 t h hour for the 10-bellow one) and tend to be stable later. The total flexion angle increments are 9.9 % and 6.0 % for the 7-bellow and the 10-bellow RFiSFAs, respectively. On the other side, there are no obvious variation trends for the blocking force of both RFiSFAs. The slight fluctuations measured are 0.017 N and 0.020 N for the 7-bellow and the 10-bellow RFiSFAs, respectively.

3. Modular design of the anthropomorphic hand

3.1. Multi-DoF fingers based on RFiSFAs

Although the human hand is reported to have more than 20 DoFs, completely imitating the actuation and transmission system of human hand may introduce difficulties in design, fabrication and control [30]. In this section, we decouple the mobility of human hand into 11 DoFs and employ the modularized RFiSFAs to construct the 2-DoF flexion finger and the 3-DoF thumb. Note that index, middle, ring and little fingers share the same finger type, i.e., the 2-DoF flexion finger.

Fig. 8(a) illustrates the 2-DoF flexion finger consisting of two serially linked 7-bellow RFiSFAs. These two RFiSFAs are responsible for flexion motions at MCP joint and PIP joint, respectively. MCP joint and PIP joint are underactuated with an internal air channel and hence only one air inlet is reserved for tube connection. The distal interphalangeal (DIP) joint is passive and integrated with the fingertip, which is designed as an interactive flexible interface with the environment.

Fig. 8(b) illustrates the 3-DoF thumb consisting of two parallel 10-bellow RFiSFAs and two serial 7-bellow RFiSFAs. It performs

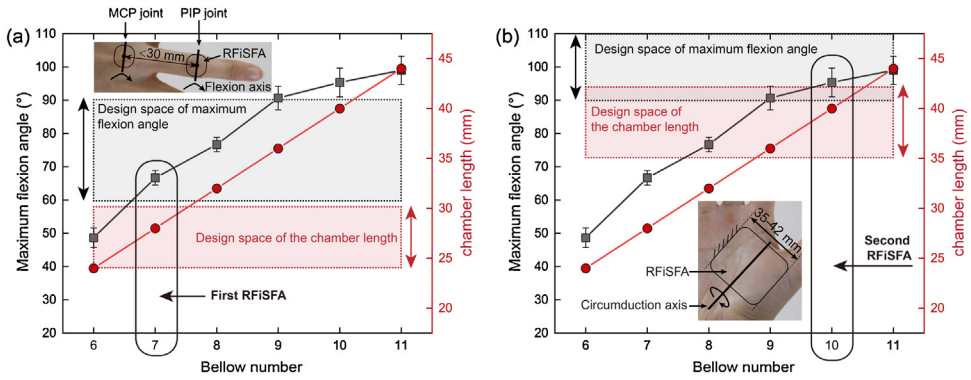

Fig. 6. Design spaces of the maximum flexion angle and the chamber length. (a) Selection of the first RFiSFA. (b) Selection of the second RFiSFA.

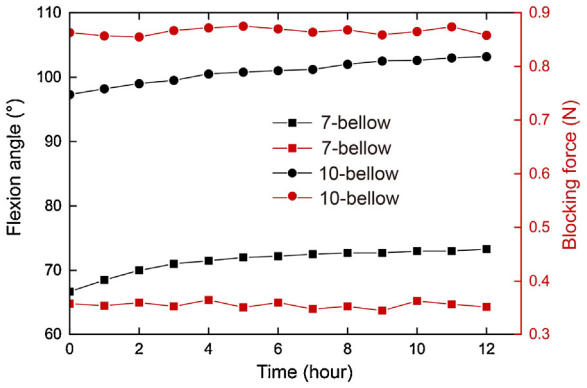

Fig. 7. The flexion angle and the blocking force of the selected RFiSFAs plotted as a function of time.

circumduction, adduction and flexion motions from the proximal end to the distal end. Firstly, two parallel 10-bellow RFiSFAs form the circumduction unit which is fixed on the palm skeleton with an incidence angle of 30°. The circumduction unit flex around the palm axis to help palm opposition. The parallel arrangement also increases the stiffness of the whole thumb. Secondly, the adduction unit is a 7-bellow RFiSFA that compels the thumb to bend inward, which is responsible for lateral pinch. Its rotational axis is perpendicular to that of the circumduction unit. In our design, the active circumduction unit and adduction unit approximatively replicate the function of the human's carpometacarpal (CMC) joint with non-intersecting motion axes. Thirdly, the flexion unit is designed with a 7-bellow RFiSFA that acts as the MCP joint. It has an inclination angle of 10° with that of the adduction unit to enhance the grasp capability. Finally, the interphalangeal (IP) joint is passive and integrated with the thumb tip. Three air inlets are reserved for tube connection. Note that we design anchor holes on the bases of the 2-DoF flexion finger and the 3-DoF thumb for the quick assembly. Similarly, corresponding anchor holes are reserved on the palm skeleton.

3.2. Anthropomorphic hand

As shown in Fig. 9(a), we develop the anthropomorphic hand mechanism based on three classes of components: active joints generated with RFiSFAs (green), flexible fingertips and passive joints with pure flexible materials (yellow), and the rigid skeletons (grey). The designed 11-DoF anthropomorphic hand integrating one thumb and four flexion fingers is driven by total 12 RFiSFAs. We also design customized architectures for quick assembly of fingers and the base skeleton, which provides improved replaceability compared to other 3D-printed soft hands [18]. Through this way, we simplify and reconstruct the biological structure and motion of human hand in an anthropomorphic form.

The overall printing time is about 5 h. In the post process, we manually remove the support materials coating the inner and external surface of the printed models mildly to avoid scratch. Next, we regulate the water pressure of the WaterJet cleaning station for

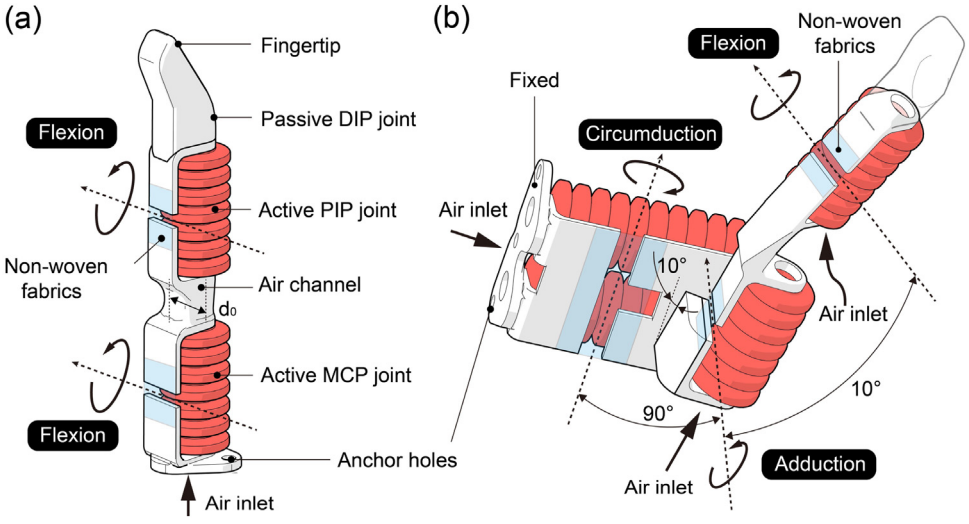

Fig. 8. Modularized design of fingers. (a) The 2-DoF flexion finger. (b) The 3-DoF thumb.

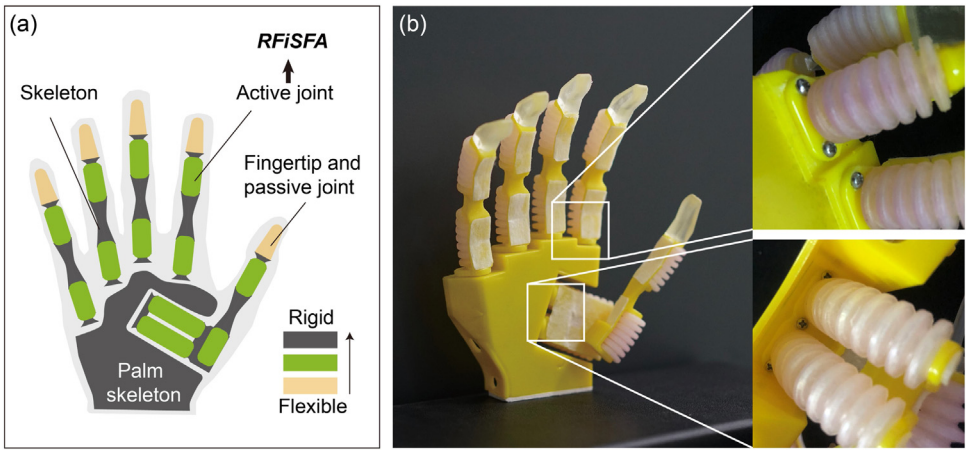

Fig. 9. Design, fabrication and assembly of the anthropomorphic hand. (a) Schematic illustration of an anthropomorphic hand integrating three classes of components: active joints generated with RFiSFAs (green), flexible fingertips and passive joints with pure flexible materials (yellow), and the rigid skeletons (grey). (b) Prototype of the fabricated anthropomorphic hand and assembly connections. (For interpretation of the references to colour in this figure legend, the reader is referred to the web version of this article).

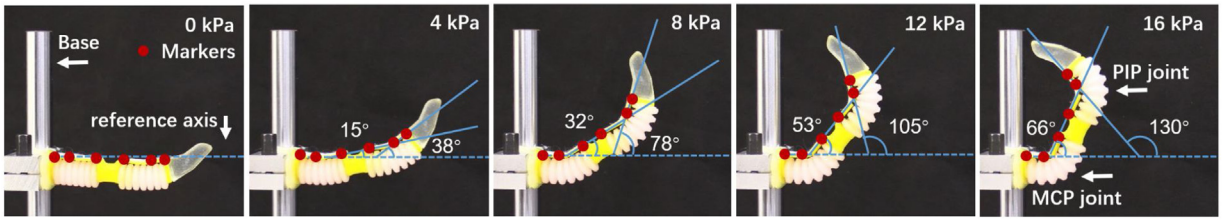

Fig. 10. Still image of the flexion motion of a 2-DoF finger.

deeper support material removal. The fabrics are then attached to the joint levers as described in Section 2.3 and air tubes are attached to the air inlets to generate airtight fingers. Finally, we use threaded connections to assemble the fingers to the palm skeleton within a few minutes (Fig. 9(b)).

4. Evaluation of the motion and force performance

4.1. Characterization of the flexion angle

In this section, we test the flexion angles of the 2-DoF fingers over increasing supplied pressures. Since the 3-DoF thumb has different rotation axes, its mobility is not quantitatively characterized and compared with other fingers in this work. As shown in Fig. 10, we attach 6 markers on the finger base, the levers of MCP joint, and the levers of PIP joint, respectively. For the 2-DoF finger, the DIP joint and fingertip are passive which can be regarded as a rigid body in the procedure. Therefore, the positions of markers on the distal end of the PIP joint lever can also be used to calculate the flexion angle of the fingertip. The experiments are performed for three times, and the results are averaged. As shown in Fig. 11(a), the maximum flexion angles of MCP joint and fingertip reach 66° and 130° at the maximum tolerable air pressure (16 kPa). The error bar indicates the standard deviation of the flexion angle. The curves are approximately linear, which is conducive to position control of fingers. Furthermore, the slope of fingertip fitting curve (8.31) is almost two times of that of MCP joint (4.41), which shows good coherence of the two serially linked RFiSFAs. To furtherly explore the consistency between the four fingers, we calculate the relative error variations of the flexion angles (Fig. 11(b)). The relative error at a certain supplied pressure is calculated by $e = \Delta\theta/\theta_0$, where $\Delta\theta$ is the standard deviation of the flexion angle and θ_0 is the average flexion angle of the four fingers. The results show that both relative errors for the MCP joint and fingertip are less than 10 % at supplied pressures from 4 kPa to 16 kPa. At 0 kPa to 4 kPa, the relative errors may exceed 10 % (to 20.2 % and 13.2 % at 2 kPa for the MCP joint and fingertip, respectively). But the absolute errors at 2 kPa reach only 1.41° and 2.16° for the two joints, which is negligible and can be attributed to measuring errors. Therefore, the results show that the fabrication process ensures good motion accuracy between the fingers.

4.2. Characterization of the blocking force

Since all the fingers are all composed of modularized 7-bellow and 10-bellow RFiSFAs, we choose the 2-DoF finger and the circumduction unit of thumb for the blocking force tests without loss of generality. Fig. 12(a) and (b) show the setups of blocking force measurement. Fig. 12(c) shows the maximum blocking forces of two test specimens reach 0.27 N and 0.86 N at 16 kPa, respectively. The relationship of blocking force and supplied pressure are nearly linear for both of the two test specimens. The slope of the fitting curve of the circumduction unit of thumb is 3.24 times of that of the index finger, which also verify the stiffness improvement of the parallel arrangement during actuation.

4.3. Performance validation of the anthropomorphic hand

The overall dimension of the fabricated hand prototype is 155 × 92 × 46 mm, which is comparable to that of a female hand. The hand mechanism weighs only 138 g due to the lightweight and modularized design. The hand prototype is attached to a pneumatic system which is composed of an air source (2–950 W-50, Outstanding Inc., China), pressure regulators (AR2000, Delixi Inc., China) and manometers (82100, AZ Inc., China). Three channels are connected to thumb and four channels to other four fingers. Coordinated finger motions can be achieved through sequential pneumatic control. Fig. 13(a) and Movie S1 show the indepen-

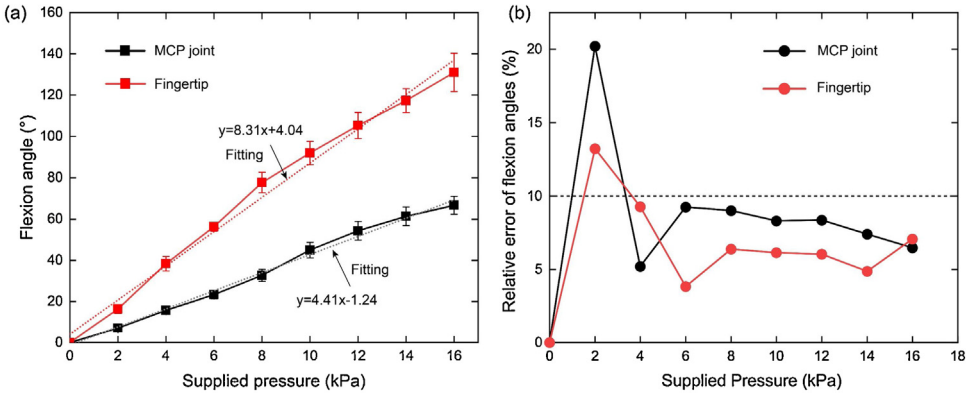

Fig. 11. Characterization of the flexion angles. (a) Flexion angles of MCP joint and fingertip. (b) Relative error of the flexion angles.

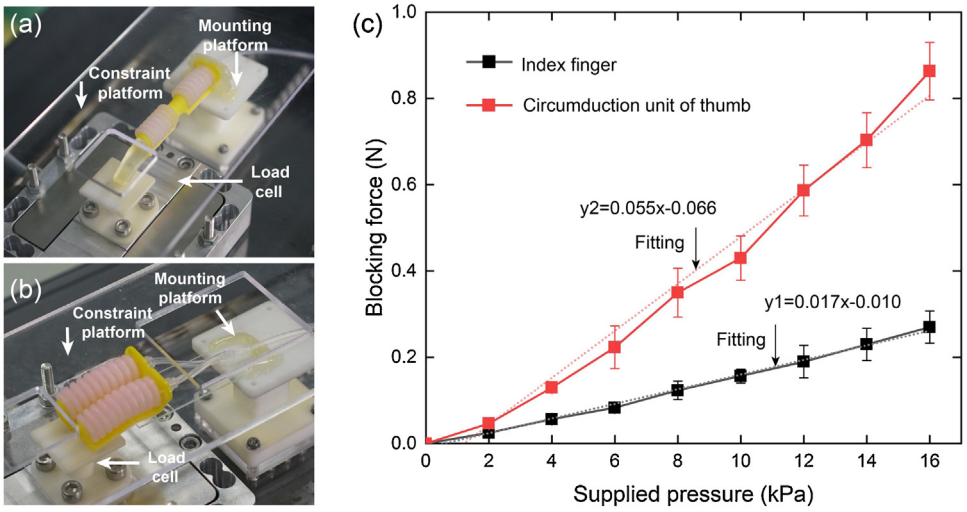

Fig. 12. Blocking force test setup for (a) the 2-DoF flexion finger and (b) the circumduction unit of thumb. (c) The blocking forces under increasing supplied air pressures.

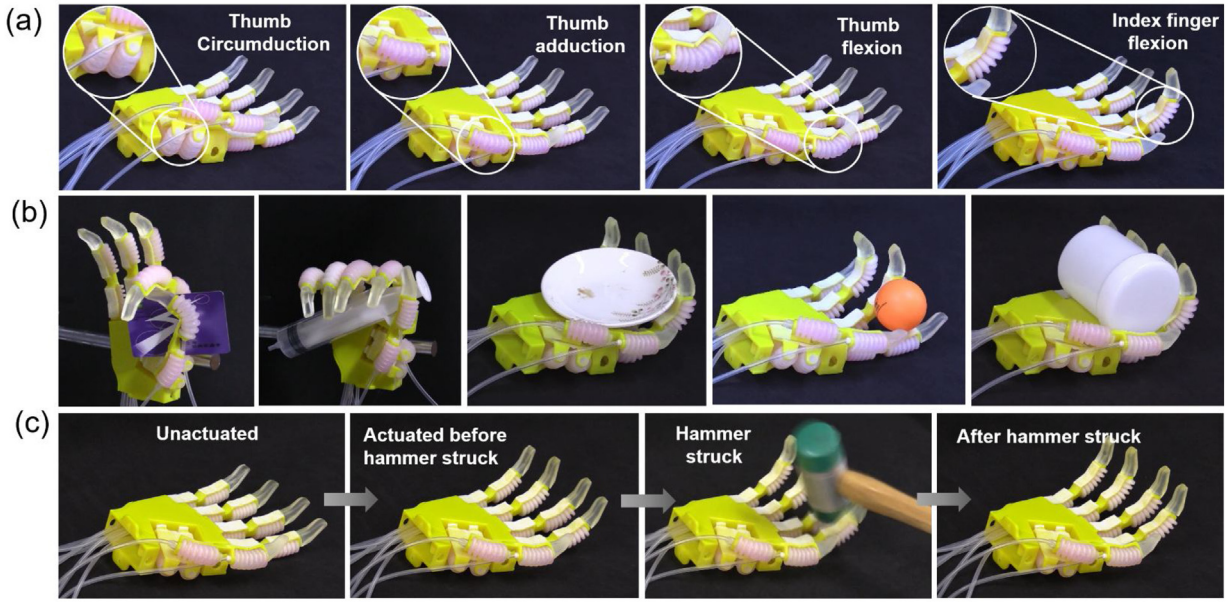

Fig. 13. Experimental demonstration of the anthropomorphic hand. (a) Independent DoFs for fingers. (b) Compliant grasping for objects with different dimensions, shapes and textures. (c) Robustness test.

Table 1
Comparison of the proposed hand with representative 3D printed, pneumatic soft hands, grippers or fingers.

	Active DoF(s)	Printing method	Printing material(s)
This work	11	Multi-material	Agilus30 series and Vero series
Three-finger soft gripper [22]	9	Multi-material	Tango Black + and Vero Clear
Soft robotic hand [18]	8	Single material	TPU
High-force soft gripper [20]	4	Single material	NinjaFlex
Antagonistic fluidic finger [19]	2	Single material	EP resin
Two-finger soft gripper [21]	2	Multi-material	Elastomer and polyethylene glycol
Anthropomorphic soft skeleton hand [29]	0	Multi-material	Tango Black and Agile White

dent motion for thumb circumduction, thumb adduction, thumb flexion, and index finger flexion (as an example). In the grasping tests, the hand prototype is installed vertically or horizontally on the base. We synchronously control the pressure regulators for the fingers. As shown in Fig. 13(b), the anthropomorphic hand is capable of grasping objects with different dimensions, shapes and textures (Movie S1). The hand's inherent compliance provides adaptive envelop of objects and rigid skeletons provide sufficient support for objects weighting below 50 g. The load capability can be furtherly improved by developed materials and optimal topological structures in future works. Finally, the robustness test shows that the hand is able to withstand the vertical impact of the hammer struck and still work well without air leakages or damages (Fig. 13(c) and Movie S1), which attributes to the inherent flexibility of the digital materials and tight connections between printable components.

In Table 1, we also compare our developed hand with existing 3D printed, pneumatic soft hands, grippers or fingers in the literature, in terms of active DoFs, printing method and printing materials. The results indicate that our hand has more active DoFs than others due to the modular and compact design approach. Among the diverse printing methods, the multi-material method is popular mainly because it introduces multiple materials with a range of mechanical performances. In addition, it is worthy of noting that the flexible bellow chamber can also be fabricated by the traditional molding method [15,33]. However, the additionally manual assembly of the joint levers to a sealed system is required.

5. Conclusions

In this paper, we present pneumatical, multi-material 3D printed, modularized RFiSFAs that can be directly utilized to build anthropomorphic hands. The RFiSFA has a bellow chamber and joint mechanisms with seamless connections. The experiment results show the influence of the chamber material and the bellow number on the burst pressure, the flexion angle, the blocking force and the chamber length of the RFiSFA. Based on the experiment results, we select the 60A material as the chamber material, and 7-bellow and 11-bellow RFiSFAs for different parts of an anthropomorphic hand. Two classes of fingers are designed, in which the 3-DoF thumb has two parallel RFiSFAs and two serial RFiSFAs, and the 2-DoF flexion finger has two serial RFiSFAs. For the 2-DoF finger, the flexion angle increases with increasing supplied pressure in a nearly linear manner and the maximum flexion angle of fingertip reaches 130° at the supplied pressure of 16 kPa. The errors of flexion angles between four 2-DoF flexion fingers are relatively small (less than 2.16° at 0∼4 kPa for the absolute error and less than 10 % at 4 ∼16 kPa for the relative error). The parallel thumb circumduction unit has a larger blocking force output and actuation stiffness (0.86 N, 55 mN/kPa) than that of the 2-DoF flexion finger (0.27 N, 17 mN/kPa). An 11-DoF anthropomorphic hand (dimension: 155 × 92 × 46 mm, weight: 138 g) is directly assembled with RFiSFA-based fingers. In the grasping experiment, the fabricated hand is able to grasp objects with different dimensions, shapes and textures. In the robustness tests, the proposed hand is able to withstand proper impacts of the hammer struck without air leakage or damage.

There also remains some potential aspects to improve the RFiSFA. Firstly, the payload of the RFiSFA is insufficient for objects with larger mass. We believe that the development in mechanical properties (tensile strength, tear resistance, fatigue life) of the printable flexible material will make the printable RFiSFA for more practical application. Secondly, the joint "ligament" that we expect is flexible but inextensible. However, there is no such material in our Polyjet system for the current version and we use non-woven fabrics instead as a compromise. Thirdly, the cost of the multi-material Polyjet printing is still high. Despite of these challenges that we encounter, this work provides an alternative method to design and fabricate the anthropomorphic hands with integrated rigid-flexible structures, which may be utilized for prosthetic hands in the future. Furthermore, with the development of 3D printing technologies including material performance and reduced cost, other 3D printed robots, especially bioinspired ones that contains modularized rigid-flexible component and multiple DoFs will meet prosperous development in the future.

Declaration of Competing Interest

None.

CRediT authorship contribution statement

Ningbin Zhang: Methodology, Investigation, Formal analysis, Visualization, Writing - original draft, Writing - review & editing. **Lisen Ge:** Methodology, Investigation. **Haipeng Xu:** Methodology, Investigation. **Xiangyang Zhu:** Supervision, Conceptualization, Project administration, Funding acquisition, Writing - original draft, Writing - review & editing. **Guoying Gu:** Supervision, Conceptualization, Project administration, Funding acquisition, Writing - original draft, Writing - review & editing.

Acknowledgements

This work was supported by the National Natural Science Foundation of China (Nos 51620105002 and 91848204).

Appendix A. Supplementary data

Supplementary material related to this article can be found, in the online version, at doi:https://doi.org/10.1016/j.sna.2020.112090.

References

[1] C. Piazza, G. Grioli, M. Catalano, A. Bicchi, A century of robotic hands, Annu. Rev. Control Robot. Auton. Syst. 2 (2019) 1–32.
[2] A. Billard, D. Kragic, Trends and challenges in robot manipulation, Science 364 (6446) (2019), eaat8414.

[3] L. Birglen, T. Laliberté, C. Gosselin, Underactuated Robotic Hands, Springer Tracts in Advanced Robotics, Springer Verlag, Berlin, Heidelberg, 2008.
[4] M. Gabiccini, E. Farnioli, A. Bicchi, Grasp analysis tools for synergistic underactuated robotic hands, Int. J. Robot. Res. 32 (13) (2013) 1553–1576.
[5] A.M. Dollar, R.D. Howe, The highly adaptive SDM hand: design and performance evaluation, Int. J. Robot. Res. 29 (5) (2010) 585–597.
[6] C. Brown, H. Asada, Inter-finger coordination and postural synergies in robot hands via mechanical implementation of principal components analysis, Intelligent Robots and Systems (IROS), IEEE/RSJ International Conference on (2007), IEEE/RSJ 2007.
[7] M.G. Catalano, G. Grioli, E. Farnioli, A. Serio, C. Piazza, A. Bicchi, Adaptive synergies for the design and control of the Pisa/IIT SoftHand, Int. J. Robot. Res. 33 (5) (2014) 768–782.
[8] S. Li, X. Sheng, H. Liu, X. Zhu, Design of a myoelectric prosthetic hand implementing postural synergy mechanically, Indu. Robot: Int. J. 41 (5) (2014) 447–455.
[9] C. Laschi, B. Mazzolai, M. Cianchetti, Soft robotics: technologies and systems pushing the boundaries of robot abilities, Sci. Robot. 1 (1) (2016), eaah3690.
[10] J. Shintake, V. Cacucciolo, D. Floreano, H. Shea, Soft robotic grippers, Adv. Mater. 30 (29) (2018), 1707035.
[11] G. Bao, L. Pan, H. Fang, X. Wu, H. Yu, S. Cai, B. Yu, Y. Wan, Academic review and perspectives on robotic exoskeletons, IEEE Trans. Neur. Sys. Reh. 27 (11) (2019) 2294–2304.
[12] E. Brown, N. Rodenberg, J. Amend, A. Mozeika, E. Steltz, M.R. Zakin, H. Lipson, H.M. Jaeger, Universal robotic gripper based on the jamming of granular material, Natl. Acad. Sci. U. S. A. 107 (44) (2010) 18809–18814.
[13] K. Kim, X. Liu, Y. Zhang, Y. Sun, Nanonewton force-controlled manipulation of biological cells using a monolithic MEMS microgripper with two-axis force feedback, J. Micromech. Microeng. 18 (5) (2008), 055013.
[14] Z. Xie, A.G. Domel, N. An, C. Green, Z. Gong, T. Wang, E.M. Knubben, J.C. Weaver, K. Bertoldi, L. Wen, Octopus arm-inspired tapered soft actuators with suckers for improved grasping, Soft Robot. (2020).
[15] K.C. Galloway, K.P. Becker, B. Phillips, J. Kirby, S. Licht, D. Tchernov, R.J. Wood, D.F. Gruber, Soft robotic grippers for biological sampling on deep reefs, Soft Robot. 3 (1) (2016) 23–33.
[16] O.Brock Deimel, A novel type of compliant and underactuated robotic hand for dexterous grasping, Int. J. Robot. Res. 35 (1-3) (2016) 161–185.
[17] J. Zhou, X. Chen, U. Chang, J.T. Lu, C.C.Y. Leung, Y. Chen, Y. Hu, Z. Wang, A soft-robotic approach to anthropomorphic robotic hand dexterity, IEEE Access 7 (2019) 101483–101495.
[18] R.B.N. Scharff, E.L. Doubrovski, W.A. Poelman, P.P. Jonker, C.C.L. Wang, J.M.P. Geraedts, Towards Behavior Design of a 3D-Printed Soft Robotic Hand, Soft Robotics: Trends, Applications and Challenges, Springer, 2017.
[19] T.J. Wallin, J.H. Pikul, S. Bodkhe, B.N. Peele, B.C. MacMurray, D. Therriault, B.W. Mcenerney, R.P. Dillon, E.P. Giannelis, R.F. Shepherd, Click chemistry stereolithography for soft robots that self-heal, J. Mater. Chem. B 5 (31) (2017) 6249–6255.
[20] K.Y. Hong, Y.N. Hui, C.H. Yeow, High-force soft printable pneumatics for soft robotic applications, Soft Robot. 3 (3) (2016) 144–158.
[21] R. MacCurdy, R. Katzschmann, Y. Kim, D. Rus, Printable hydraulics: a method for fabricating robots by 3D co-printing solids and liquids, in: Robotics and Automation (ICRA), IEEE International Conference on, 2016, IEEE, 2016.
[22] D. Drotman, M. Ishida, S. Jadhav, M.T. Tolley, Application-driven design of soft, 3-D printed, pneumatic actuators with bellows, IEEE-ASME Trans. Mech. 24 (1) (2019) 78–87.
[23] M.A. Skylar-Scott, J. Mueller, C.W. Visser, J.A. Lewis, Voxelated soft matter via multimaterial multinozzle 3D printing, Nature 575 (7782) (2019) 330–335.
[24] N.W. Bartlett, M.T. Tolley, J.T. Overvelde, J.C. Weaver, B. Mosadegh, K. Bertoldi, G.M. Whitesides, R.J. Wood, A 3D-printed, functionally graded soft robot powered by combustion, Science 349 (6244) (2015) 161–165.
[25] K. Kumar, J. Liu, C. Christianson, M. Ali, M.T. Tolley, J. Aizenberg, D.E. Ingber, J.C. Weaver, K. Bertoldi, A biologically inspired, functionally graded end effector for soft robotics applications, Soft Robot. 4 (4) (2017) 317–323.
[26] L.K. Ma, Y. Zhang, Y. Liu, K. Zhou, X. Tong, Computational design and fabrication of soft pneumatic objects with desired deformations, ACM Trans. Graphic 36 (6) (2017) 1–12.
[27] M. Schaffner, J. Faber, L. Pianegonda, P.A. Ruhs, F. Coulter, A.R. Studart, 3D printing of robotic soft actuators with programmable bioinspired architectures, Nat. Commun. 9 (1) (2018) 878.
[28] Y.F. Zhang, N. Zhang, H. Hingorani, N. Ding, D. Wang, C. Yuan, B. Zhang, G. Gu, Q. Ge, Fast-response, stiffness-tunable soft actuator by hybrid multimaterial 3D printing, Adv. Funct. Mater. 29 (15) (2019), 1806698.
[29] J.A.E. Hughes, P. Maiolino, F. Iida, An anthropomorphic soft skeleton hand exploiting conditional models for piano playing, Sci. Robot. 3 (25) (2018), eaau3098.
[30] P.W. Brand, A.M. Hollister, Clinical Mechanics of the Hand, 3rd ed., Mosby, St. Louis, MO, 1999.
[31] G. Dämmer, S. Gablenz, A. Hildebrandt, Z. Major, PolyJet-printed bellows actuators: design, structural optimization, and experimental investigation, Front. Robot. AI 6 (34) (2019).
[32] https://www.stratasys.com/.
[33] B. Mosadegh, P. Polygerinos, C. Keplinger, S. Wennstedt, R.F. Shepherd, U. Gupta, J. Shim, K. Bertoldi, C.J. Walsh, G.M. Whitesides, Pneumatic networks for soft robotics that actuate rapidly, Adv. Funct. Mater. 24 (15) (2014) 2163–2170.

Biographies

Ningbin Zhang received the B.E. degree in mechanical engineering and M.S. degree in mechatronic engineering from Zhejiang Sci-Tech University, Hangzhou, China, in 2012 and 2016, respectively. He is currently a Ph.D. candidate at School of Mechanical Engineering, Shanghai Jiao Tong University. His research is in the development of soft robotics.

Lisen Ge received the B.E. degree in Engineering Structure Analysis and M.S. degree in Vehicle Operation Engineering from Southwest Jiaotong University, Chengdu, China, in 2013 and 2016, respectively. He is currently a Ph.D. candidate at School of Mechanical Engineering, Shanghai Jiao Tong University, Shanghai, China. His research is in the development of soft robotics.

Haipeng Xu received the B.S. degree (with honors) in mechanical engineering from Northeastern University, Shenyang, China, in 2017. He is currently working toward the Ph.D. degree in mechanical engineering with Shanghai Jiao Tong University, Shanghai, China. His research interests include 3D-printing soft sensors and robots.

Xiangyang Zhu received the B.S. degree from the Department of Automatic Control Engineering, Nanjing Institute of Technology, Nanjing, China, in 1985, the M.Phil. degree in instrumentation engineering and the Ph.D. degree in automatic control engineering, both from the Southeast University, Nanjing, China, in 1989 and 1992, respectively. From 1993–1994, he was a Postdoctoral Research Fellow with Huazhong University of Science and Technology, Wuhan, China. He joined the Department of Mechanical Engineering as an Associate Professor, Southeast University, Dhaka, Bangladesh, in 1995. Since June 2002, he has been with the School of Mechanical Engineering, Shanghai Jiao Tong University, Shanghai, China, where he is currently a Changjiang Chair Professor and the Director of the Robotics Institute. His current research interests include robotic manipulation planning, human–machine interfacing, and biomechatronics. Dr. Zhu received the National Science Fund for Distinguished Young Scholars in 2005.

Guoying Gu received the B.E. degree (with honors) in electronic science and technology, and the Ph.D. degree (with honors) in mechatronic engineering from Shanghai Jiao Tong University, Shanghai, China, in 2006 and 2012, respectively. Since October 2012, Dr. Gu has worked at Shanghai Jiao Tong University, where he is currently appointed as a Professor of School of Mechanical Engineering. He was a Humboldt Postdoc Fellow with University of Oldenburg, Germany. He was a Visiting Scholar at Massachusetts Institute of Technology, National University of Singapore and Concordia University. His research interests include soft robotics, intelligent wearable systems, smart materials sensing, actuation and motion control. He is the author or co-author of over 80 publications, which have appeared in Science Robotics, Science Advances, IEEE/ASME Trans., Advanced Functional Materials, Soft Robotics, etc., as book chapters and in conference proceedings. Dr. Gu is the winner of multiple awards including Young Changjiang Scholar of the Ministry of Education, National Science Fund for Excellent Young Scholars, The first prize of natural science of Ministry of Education, Best Paper Award of Advanced Robotics, ICIRA 2016 and IEEE-ICIA 2011. Now he serves as Associate Editor of IEEE Transactions on Robotics. He has also served for several journals as Editorial Board Member, Topic Editor, or Guest Editor, and several international conferences/symposiums as Chair, Co-Chair, Associate Editor or Program Committee Member.